Continuous wave interband cascade lasers near 13 μm

Yixuan Shen,[1] Rui Q, Yang,[1,a)] S. D. Hawkins,[2] and A. J. Muhowski[2]

[1]School of Electrical and Computer Engineering, University of Oklahoma, Norman, OK.

[2]Sandia National Laboratories, PO Box 5800, Albuquerque, NM 87185-1085, USA

[a)]Electronic mail: Rui.q.Yang@ou.edu

Abstract

We report the demonstration of continuous-wave (cw) interband cascade lasers (ICLs) near 13 μm. The attained lasing wavelength of 13.2 μm at 92 K stands as the longest cw emission wavelength ever reported for III-V interband lasers. This achievement is attributed to the adoption of an innovative quantum well (QW) active region comprising strained $InAs_{0.5}P_{0.5}$ layers in contrast to the commonly used "W" QW active region, showing the potential of the modified QW active region with InAsP layers in improving device performance and extending wavelength coverage of ICLs.

I. INTRODUCTION

Interband cascade lasers (ICLs)[1] have become desirable, efficient mid-infrared light sources[2-9] for various applications[10-12] owing to their low power consumption, especially in the 3-4 μm wavelength region. Although high performance of ICLs has been demonstrated at room temperature up to about 6 μm, extending the high-level performance to longer wavelengths poses challenges due to factors such as a reduced wavefunction overlap in type-II quantum well (QW) active region and rapidly rising free-carrier absorption loss with increasing wavelength. The commonly used active region in the type-II ICL is a W-shaped type-II QW that is composed of AlSb/InAs/GaInSb/InAs/AlSb layers[13,14]. With this W-QW active region in an optically pumped laser, the lasing wavelength reached to 9.5 μm[15]. For ICLs with the W-QW active region and hybrid cladding layers[16] comprising an AlSb/InAs superlattice and heavily n^+-doped InAs, the lasing wavelength was recently extended to 12.2 μm in pulsed mode and 12 μm in continuous wave (cw) operation[17]. However, those long wavelength (LW) ICLs stopped lasing with a relatively low threshold current density (<300 A/cm^2), which limited their maximum operating temperature to 137 K and 106 K in pulsed and cw modes, respectively, as well as the longest wavelength that could be reached.

Recently, based on a perspective from the band structure in type-II QWs[18], we proposed and implemented an innovative QW structure comprising strained $InAs_{0.5}P_{0.5}$ barriers in the active region of type-II ICLs[19-21], which enabled lasing extended to 14.4 μm in pulsed operation at 122 K[21]. Moreover, compared to ICLs with the regular W-QW active region at similar LW wavelengths, the maximum operating temperature for ICLs with modified QW active regions was much higher (*e.g.*, 212 K vs. 137 K near 12 μm)[21],

suggesting further benefits that the new QW active region may bring. In this work, using one of the LW ICL wafers (EB7906) from prior work with an $InAs_{0.5}P_{0.5}$ containing QW active region[21], we fabricated narrow ridge (NR) devices and demonstrated their cw operation at temperatures up to 92 K at 13.2 µm, the longest wavelength in cw mode ever achieved among ICLs and III-V interband lasers.

II. EXPERIMENT

The ICL structure was grown by molecular beam epitaxy on an InAs substrate and has 23 cascade stages, each of which is composed of a QW active region sandwiched by an InAs/AlSb(As) QW electron injector and a GaSb/AlSb(As) hole injector as described in Refs. [19-21]. Every active region in this wafer EB7906 consists of a layer sequence of $AlAs_{0.11}Sb_{0.89}$/$InAs_{0.5}P_{0.5}$/InAs/$Ga_{0.65}In_{0.35}Sb$/InAs/$InAs_{0.5}P_{0.5}$, with thicknesses of 19/16/25/28/20/13 Å in the growth direction as shown in Figure 1. The ICL structure has hybrid cladding layers comprising InAs/AlSbAs superlattice layers and n^+-doped InAs layers, as detailed in Ref. [21].

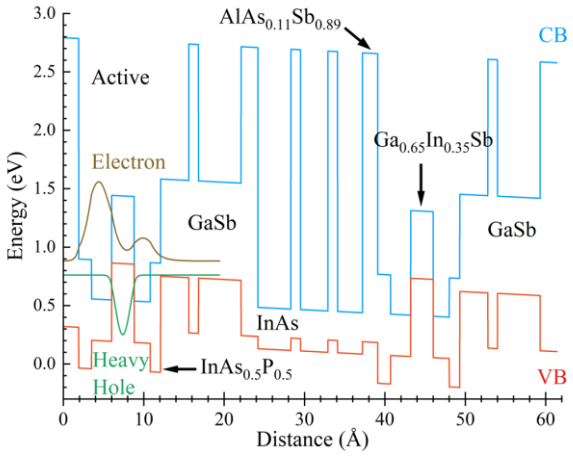

FIG. 1. Schematic band diagram of one cascade stage at 80 K and the layer sequence for wafer EB7906.

The wafer was fabricated into deep-etched narrow ridge laser devices by contact lithography and wet chemical etching to a depth of 7.1 µm. Due to substantial lateral etching, the etched ridge is a trapezoid with the narrower edge on the top. Lasers with two ridge widths were fabricated. The

average ridge widths of the cascade stages are ~8 and ~11 μm according to scanning electron microscope (SEM) measurements. The passivation layer comprises a 250-nm-thick sputtered SiO_2 layer and a thick photoresist insulating layer on top of the SiO_2 layer to prevent pinholes on the sidewalls. The contact window of the SiO_2 layer was opened by chemical etching. A 1.3-μm-thick Ti/Au contact layer was thermally deposited on the top of the wafer for current injection and improving heat dissipation. The wafer was left unthinned with a bottom metal contact and cleaved into laser bars with a 0.8- or 1.7-mm-long cavity without facet coating. Then, the laser bars were mounted epi-side-up onto copper heatsinks with indium solder for pulsed and cw testing.

Emission spectra of the fabricated ICLs were obtained using a Nicolet 8700 Fourier transform infrared spectrometer (FTIR). The cw output power was measured by a PM3 Coherent PowerMax thermopile power meter, and the pulsed output was collected by a MCT detector with a Stanford SR830 Lock-in amplifier. Since the beam divergence was large for the laser beam at long wavelengths, a portion of the beam is not counted in the cw power collection. The reported output power and external quantum efficiency (EQE) of the device are thus conservative.

III. RESULTS AND DISCUSSION

An 8-μm-wide ICL was able to lase in cw operation up to 92 K with an emission wavelength near 13.2 μm, red-shifted from 12.41 μm at 80 K, as shown in Figure 2. The significant red-shift of lasing wavelength from 80 to 92 K was caused mainly by heating in the device. This cw lasing wavelength at 92 K is significantly longer than the longest wavelength of 12.2 μm reported for ICLs with the regular W-QW active region[17], which

is also the longest cw lasing wavelength among all III-V interband lasers, indicating an enhanced wavelength tailoring capacity of ICLs with the modified QW active region. Another device with 11-µm-wide and 0.8-mm-long cavity was able to lase up to 88 K near 13 µm in cw mode, as shown in Figure 3. The cw operating temperature of 11-µm-wide and 0.8-mm-long device was 4 K lower than that of 8-µm×1.7-mm device, which might be due to a somewhat higher threshold current density J_{th} with a higher mirror loss.

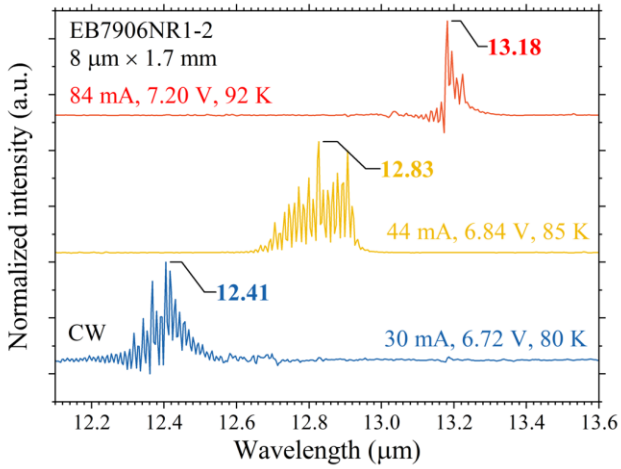

FIG. 2. Continuous wave (CW) lasing spectra of an 8 µm×1.7 mm ICL. The threshold current and voltage at each temperature are listed in the figure.

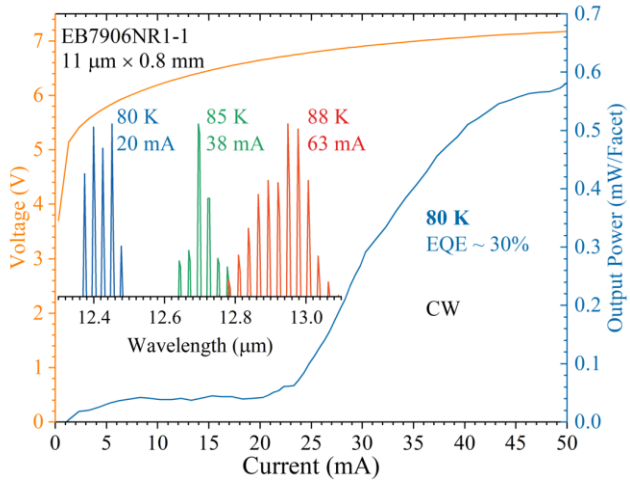

FIG. 3. Current-voltage-light (IVL) characteristics of an 11 µm×0.8 mm ICL in continuous wave (CW) mode, with its lasing spectra (inset) at several temperatures.

At 80 K, the two devices had comparable J_{th}: 225 A/cm^2 for the 8-µm×1.7-mm device and 230 A/cm^2 for the 11-µm×0.8-mm device, despite a substantial difference in cavity length and mirror loss. This might be compensated partially by the difference in leakage current through sidewalls due to different ridge widths. Although the pulsed J_{th} (205 A/cm^2 with a threshold voltage of 6.72 V at 80 K for the 11-µm-wide device in Figure 4) is slightly lower than the cw J_{th}, the J_{th} for NR devices at 80 K was more than three times the pulsed J_{th} of broad-area (BA) devices (*i.e.*, 69 A/cm^2) [21] as shown in Figure 5. The difference in J_{th} between NR and BA devices decreased with increasing temperature due to reduced device resistance at higher temperatures, which helped carrier transport across the ICL structure. This suggests that the increased J_{th} was caused mainly by a large portion of current leakage through sidewalls and extra optical loss due to optical scattering and absorption near the sidewalls with SiO_2 passivation layer, as SiO_2 has substantial absorption at this long wavelength. As a result, more electrons are required to yield a sufficient optical gain to compensate the higher loss at the threshold.

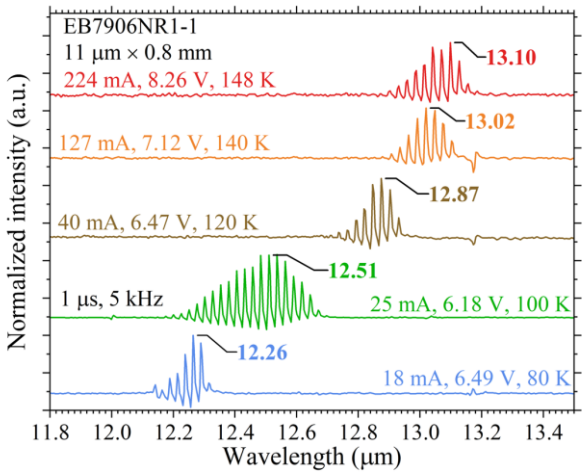

FIG. 4. Pulsed lasing spectra at various temperatures for the 11-µm-wide ICL. The threshold current and voltage at each temperature are listed in the figure.

At 80 K, the cw lasing wavelength of the NR device was 12.4 µm, 0.5 µm shorter than the lasing wavelength of 12.9 µm for the BA device in pulsed operation. The pulsed

lasing wavelength was 12.26 μm at 80 K, as shown in Figure 4, even shorter without the heating effect. This blue-shift of lasing wavelength could be caused by the combination of wafer nonuniformity and band-filling effect due to the much higher threshold current density. Nevertheless, the lasing wavelength was still in the same gain peak since the photon energy was increased only by 4.7 meV in such a long wavelength region. The cw lasing wavelength red-shifted with increasing temperature at a rate of 64.2 nm/K, much higher than 12.4 nm/K in the pulsed operation, implying significant heating in the active region. This heating made the actual device temperature substantially higher than the heat-sink temperature. For example, for the 11-μm-wide device in cw operation at 88 K, the actual temperature in its active region was about 128 K (40 K higher than 88 K), which can be extracted by comparing J_{th} in pulsed and cw modes as shown in Figure 5. Although the NR devices exhibited significant higher J_{th} compared to the BA devices, the 11-μm-wide device lased in pulsed mode at temperatures up to 148 K with a J_{th} of 2.5 kA/cm^2, only 2 K below the maximum operating temperature of 150 K for the BA devices, as shown in Figures 4 and 5.

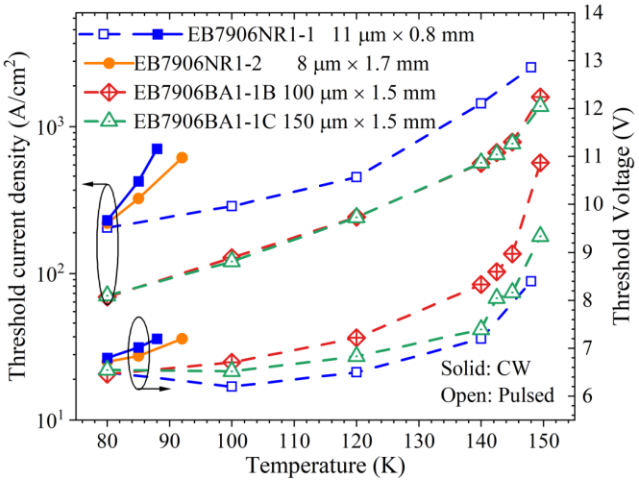

FIG. 5. Threshold current density and voltage of EB7906 for both BA and NR devices.

The pulsed lasing wavelength of the 11-µm-wide device was 0.17 µm shorter than cw lasing wavelength at 80 K, even though the input power was only 129 mW, indicating a considerable heating issue for LW ICLs due partially to both higher threshold current density and operating voltage with more cascade stages. Consequently, as shown in Figure 3 by the cw current-voltage-light (IVL) characteristics for the 11-µm-wide device, its output power quickly reached the thermal rollover with a maximum output power of 0.58 mW at 80 K at a current of 50 mA and voltage of 7 V. The 11-µm-wide device exhibited a cw EQE of only ~30% (Figure 3) compared to the pulsed EQE of ~ 49% at 80 K, as shown in Figure 6. Notably, both EQE values were significantly lower than the EQE value of 220% achieved by a 100-µm-wide BA device[21]. This significant reduction in EQE provided further evidence of the substantial leakage current and higher waveguide loss in the narrow ridge device. Unlike the BA device, where pulsed EQE was fairly stable at low temperatures, the EQE for NR device quickly decreased from 49% at 80 K to 24% at 100 K, suggesting a strong temperature dependent waveguide loss, which might be related to the optical loss at longer wavelengths.

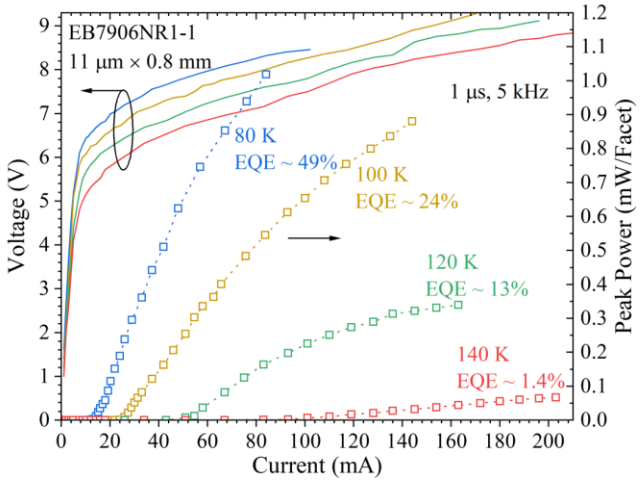

FIG. 6. IVL characteristics of the 11-µm-wide ICL in the pulsed mode.

Figure 5 summarizes the threshold current densities and threshold voltage for both BA and NR devices. The NR devices exhibited a higher J_{th} due to the current leakage

through sidewalls and extra optical loss, but their characteristic temperature T_0 of 31 K (extracted from 80 to 140 K) is comparable to the value for BA devices. The extracted thermal resistance R_{th} is ~10 Kcm^2/kW, partially due to the 1.3-μm-thick gold layer deposited on the top, which is improved compared to BA devices. The NR device had a slightly lower threshold voltage and higher voltage efficiency compared to the BA device, especially at higher temperatures as the current distribution might be easier and better in smaller devices. The voltage efficiency (η_v) is defined as $\eta_v = N_s E_p / eV_{th}$, where N_s is the number of stages, E_p is the emitted photon energy and e is electron charge. η_v evaluates how efficiently the applied threshold voltage is used to generate the quasi-Fermi energy difference in the active region for the photon energy. Hence, as their voltage efficiency (e.g., 35% at 80 K) is lower than a typical value (e.g., ~70%) that ICLs with the regular W-QW active region could achieve at shorter wavelengths, a substantial portion of the applied voltage might be consumed to overcome possible barriers in the structure, implying possible issue with carrier transport in LW ICLs with the modified QW active region, which will be a subject of our future study.

IV. SUMMARY AND CONCLUSIONS

In summary, cw operation of ICLs has been demonstrated at LW wavelengths up to 13.2 μm, indicating that a milestone was passed with the use of an innovative QW active region. While this longest ever-reported cw wavelength for ICLs suggests the promising potential of incorporating InAsP barriers in the active region, this new type of ICLs is still in the early stage and far from optimized as the device exhibited notably lower voltage efficiency compared to the regular “W”-QW structures and significant

optical loss and current leakage. Continued effort will be required in device fabrication and understanding to improve the performance, pushing the LW ICLs to operate at higher temperatures and for practical applications. Other quantum engineering techniques, such as mitigating inter-valence-subband transition absorption loss, which has been proven successfully in ICLs in the 4-7 μm wavelength region[6,7], can also be explored in LW ICLs with the modified QW active region for further improvements.

ACKNOWLEDGMENTS

The work at the University of Oklahoma was partially supported by NSF (No. ECCS-1931193). This work was performed, in part, at the Center for Integrated Nanotechnologies, an Office of Science User Facility operated for the U.S. Department of Energy (DOE) Office of Science. This article has been authored by an employee of National Technology & Engineering Solutions of Sandia, LLC under Contract No. DE-NA0003525 with the U.S. Department of Energy (DOE). The employee owns all right, title and interest in and to the article and is solely responsible for its contents. The United States Government retains and the publisher, by accepting the article for publication, acknowledges that the United States Government retains a non-exclusive, paid-up, irrevocable, world-wide license to publish or reproduce the published form of this article or allow others to do so, for United States Government purposes. The DOE will provide public access to these results of federally sponsored research in accordance with the DOE Public Access Plan https://www.energy.gov/downloads/doe-public-access-plan. We thank Zhisheng Shi for lending a MCT detector used for the pulsed power measurment.

AUTHOR DECLARATIONS

The authors have no conflicts to disclose.

DATA AVAILABILITY

Data available upon reasonable request from the authors.

REFERENCES

[1] R. Q. Yang, Superlattices Microstruct. **17**, 77 (1995).

[2] I. Vurgaftman, R. Weih, M. Kamp, J. R. Meyer, C. L. Canedy, C. S. Kim, M. Kim, W. W. Bewley, C. D. Merritt, and J. Abell, J. Phys. D: Appl. Phys. **48** 123001 (2015).

[3] J. Koeth, R. Weih, J. Scheuermann, M. Fischer, A. Schade, M. Kamp, and S. Höfling, Proc. SPIE, **10403**, 1040308 (2017).

[4] R. Q. Yang, L. Li, W. Huang, S. M. Shazzad Rassel, J. A. Gupta, A. Bezinger, X. Wu, G. Razavipour, and G. C. Aers, IEEE J. Sel. Top. Quant. Electron., **25**, 1200108 (2019).

[5] J. R. Meyer, W. W. Bewley, C. L. Canedy, C. S. Kim, M. Kim, C. D. Merritt, and I. Vurgaftman, Photonics, **7**, 75 (2020).

[6] H. Knotig, J. Nauschutz, N. Opacak, S. Hofling, J. Koeth, R. Weih, and B. Schwarz, Laser & Photonics Reviews, 2200156 (2022).

[7] J. Nauschutz, H. Knotig, R. Weih, J. Scheuermann, J. Koeth, S. Hofling, and B. Schwarz, Laser & Photonics Reviews, 2200587 (2023).

[8] K. Zhang, Y. Lin, W. Zheng, R. Q. Yang, H. Lu and Y. F. Chen, J. Crystal Growth, **586**, 1266185 (2022).

[9] W. Huang, S. Hu, J. Tu, L. Zhang, K. Tao, and P. Wang, Appl. Phys. Lett, **123**, 151111 (2023).

[10] J. Scheuerman., P. Klucynski, K. Siembab, M. Straszewski, J. Kaczmarek, R. Weih, M. Fischer, J. Koeth, A. Schade, and S. Höfling, Appl. Spectrosc. **75**(3), 336–342 (2021)

[11] R. De Palo, A. Elefante, G. Biagi, F. Paciolla, R. Weih, V. Villada, A. Zifarelli, M. Giglio, A. Sampaolo, V. Spagnolo, and P. Patimisco, Adv. Photonics Res. **4**(6), 2200353 (2023).

[12] P. Didier, H. Knötig, O. Spitz, L. Cerutti, A. Lardschneider, E. Awwad, D. Diaz-Thomas, A. N. Baranov, R. Weih, J. Koeth, B. Schwarz, and F. Grillot, Photon. Res. **11**, 582 (2023).

[13] L. Esaki, L. L. Chang, and E. E. Mendez, Jpn. J. Appl. Phys., **20**, L529 (1981).

[14] J. R. Meyer, C. A. Hoffman, F. J. Bartoli, and L. R. Ram-Mohan, Appl. Phys. Lett., **67**, 757 (1995).

[15] A. P. Ongstad, R. Kaspi, G. C. Dente, M. L. Tilton, R. Barresi, and J. R. Chavez, Appl. Phys. Lett. **92**, 141106 (2008).

[16] L. Li, Y. Jiang, H. Ye, R. Q. Yang, T. D. Mishima, M. B. Santos, and M. B. Johnson, Appl. Phys. Lett, **106**, 251102 (2015).

[17] J. A. Massengale, Y. Shen, R. Q. Yang, S. D. Hawkins, and A. J. Muhowski, in IEEE Journal of Quantum Electronics, **59**, no. 6, 2000507 (2023).

[18] R. Q. Yang, J. Appl. Phys. **127**, 025705 (2020).

[19] J. A. Massengale, Y. Shen, R. Q. Yang, S. D. Hawkins, and J. F. Klem, Appl. Phys. Lett. **120**, 091105 (2022).

[20] J. A. Massengale, Y. Shen, R. Q. Yang, S. D. Hawkins, and J. F. Klem, Semicond. Sci. Technol. **38**, 025009 (2023).

[21] Y. Shen, J. A. Massengale, R. Q. Yang, S. D. Hawkins, and A. J. Muhowski, Appl. Phys. Lett. **123**, 041108 (2023).

Figure Captions

FIG. 1. Schematic band diagram of one cascade stage at 80 K and the layer sequence for wafer EB7906.

FIG. 2. Continuous wave (CW) lasing spectra of an 8 μm×1.7 mm ICL. The threshold current and voltage at each temperature are listed in the figure.

FIG. 3. Current-voltage-light (IVL) characteristics of an 11 μm×0.8 mm ICL in continuous wave (CW) mode, with its lasing spectra (inset) at several temperatures.

FIG. 4. Pulsed lasing spectra at various temperatures for the 11-μm-wide ICL. The threshold current and voltage at each temperature are listed in the figure.

Fig. 5. Threshold current density and voltage of EB7906 for both BA and NR devices.

Fig. 6. IVL characteristics of the 11-μm-wide ICL in the pulsed mode.